

Supporting information

Excimer Ultraviolet-Irradiated Exfoliated Graphite Loaded with Carbon-Coated SnO_x Small Nanoparticles as Advanced Anodes for High-Rate-Capacity Lithium-Ion Batteries

Zhen Shen^{a,b}, Yi Hu^{*,a,b,c}, Renzhong Chen^{a,b}, Xia He^{a,b}, Keshi Wu^{a,b}, Zhongling Cheng^{a,b}, Peng Pan^{a,b}, Liyuan Jiang^{a,b}, Jieting Mao^{a,b}, Changke Ni^{a,b}

^aKey Laboratory of Advanced Textile Materials and Manufacturing Technology Ministry of Education, Zhejiang Sci-Tech University, Hangzhou 310018, P. R. China

^bEngineering Research Center for Eco-Dying & Finishing of Textiles Ministry of Education, Zhejiang Sci-Tech University, Hangzhou 310018, P. R. China

^cDyeing and Finishing Institute of Zhejiang Sci-Tech University, Zhejiang Sci-Tech University, Hangzhou 310018, P. R. China

*Corresponding Author: Yi Hu

928 Second Avenue, Xiasha Higher Education Zone, Hangzhou, China, 310018

Phone: 86+13588321680

E-mail address: huyi-v@zstu.edu.cn

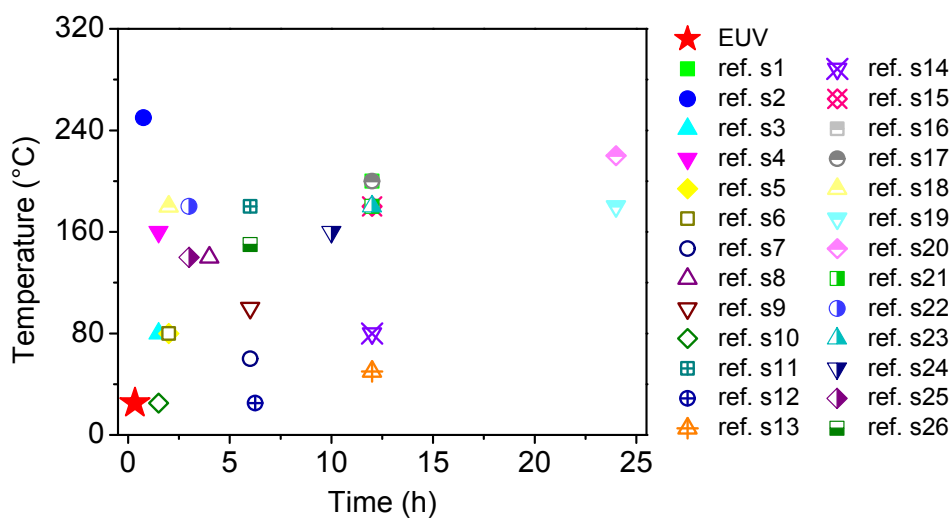


Fig. S1 Time vs. temperature of the process of SnO₂ SNPs deposition onto graphene/ exfoliated graphite in previous reports and this work.

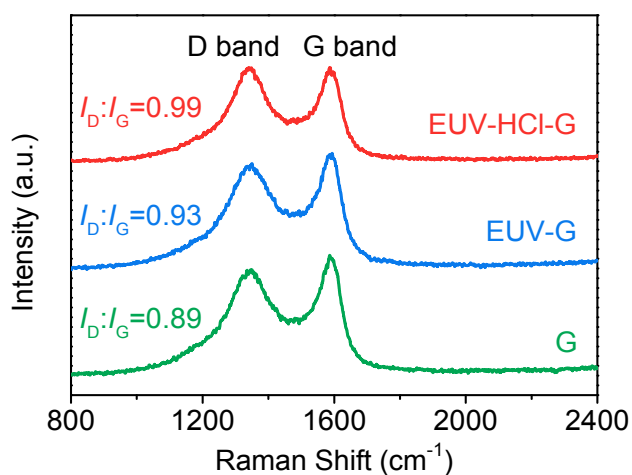


Fig. S2 Raman spectra of EUV-HCl-G, EUV-G, and exfoliated graphite.

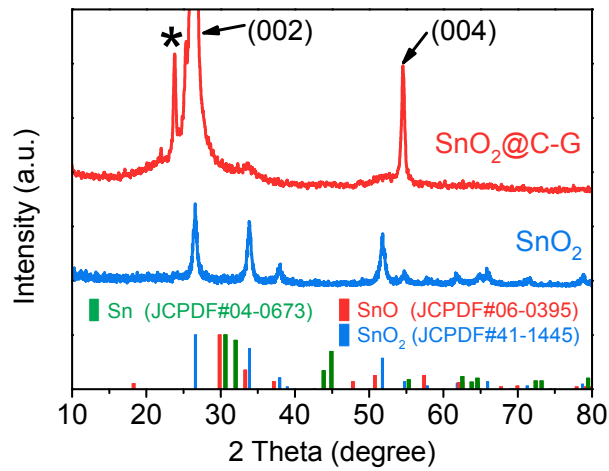


Fig. S3 XRD patterns of SnO₂@C-G and SnO₂ powders.

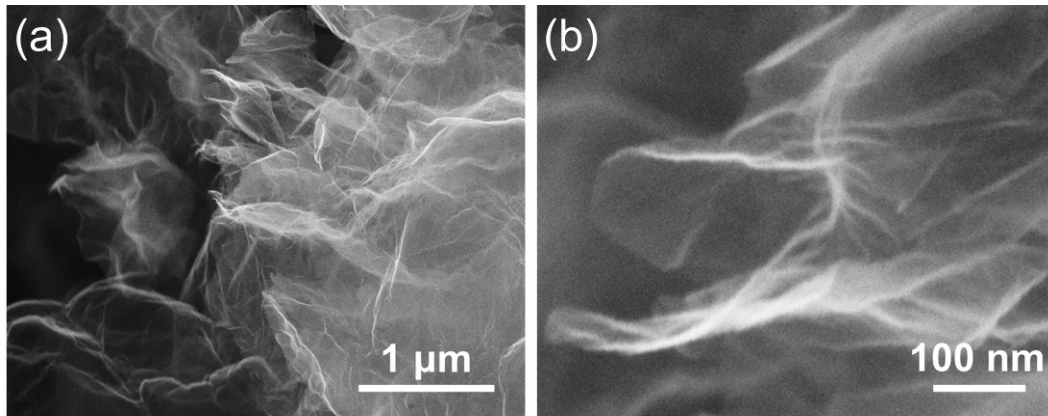


Fig. S4 SEM images of exfoliated graphite.

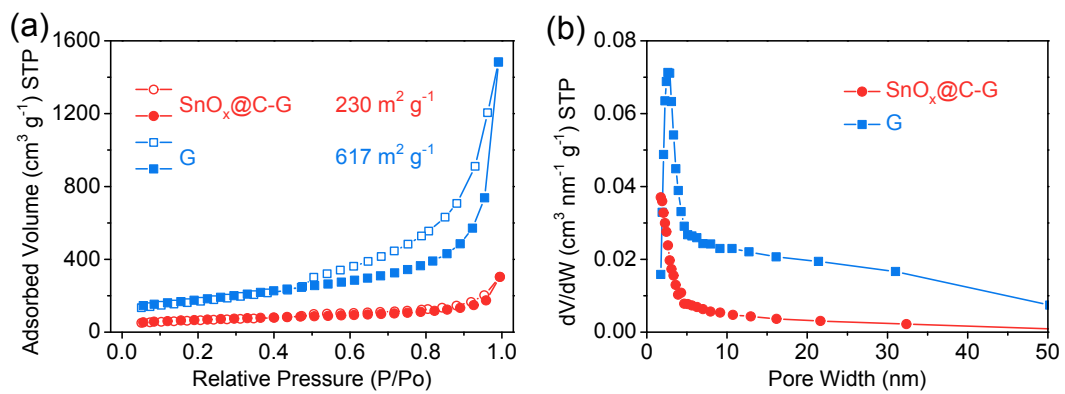


Fig. S5 (a) N₂ adsorption-desorption isotherms and (b) BJH pore distribution of SnO_x@C-G and exfoliated graphite.

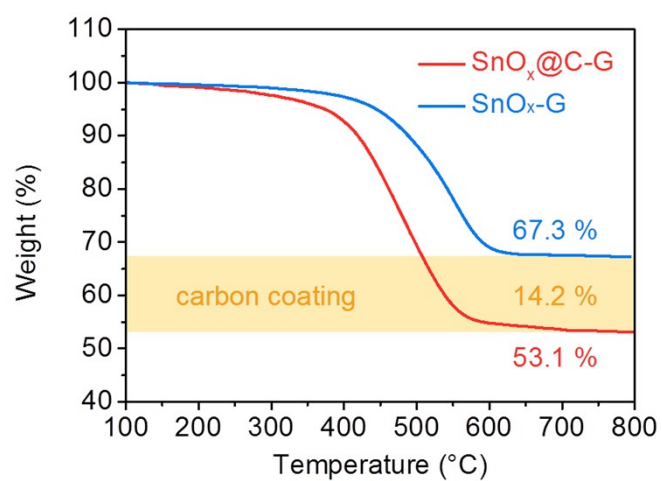


Fig. S6 TG curves of SnO_x@C-G and SnO_x-G in air recorded at a heating rate of 10 °C min⁻¹.

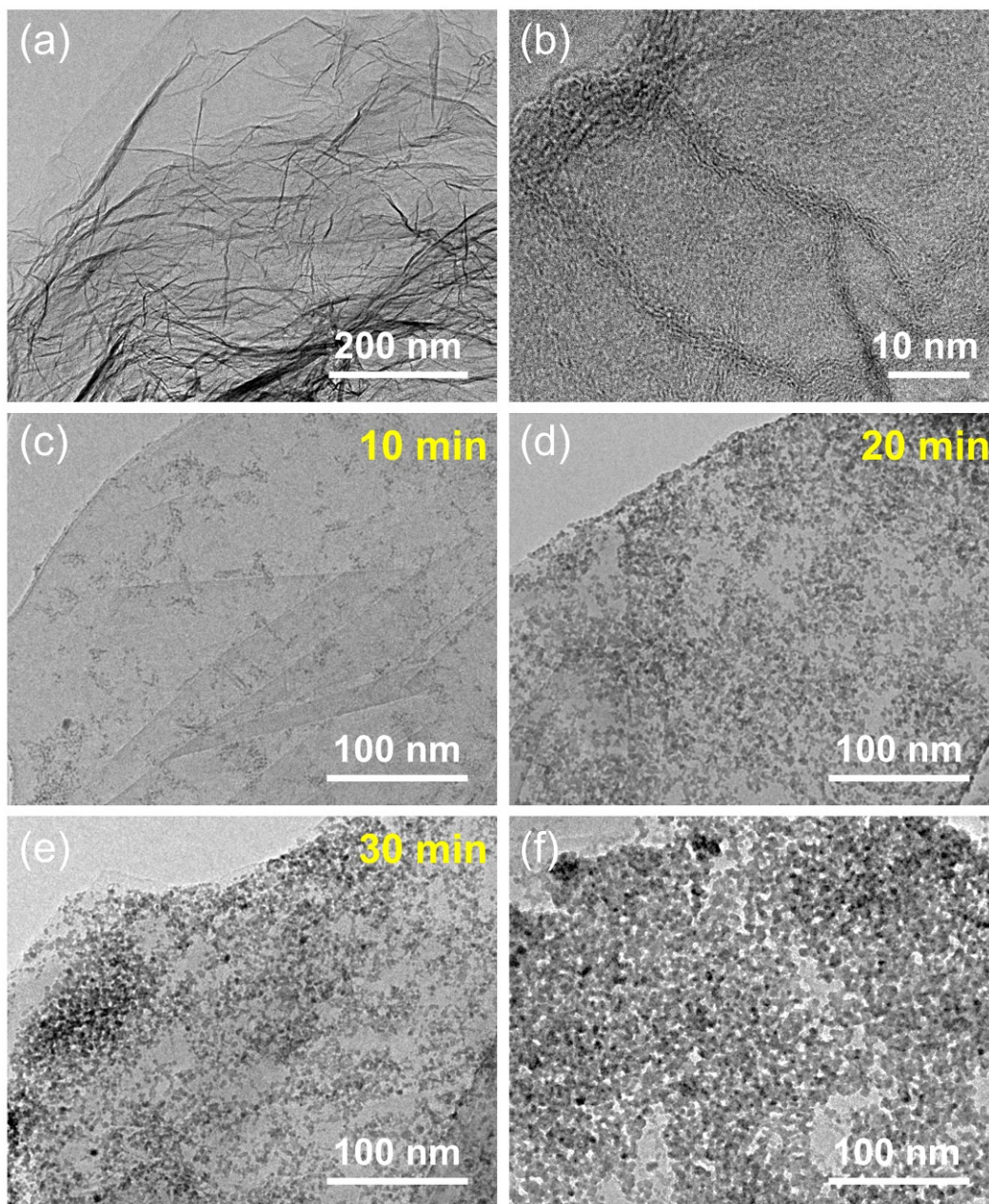


Fig. S7 (a, b) TEM images of exfoliated graphite. TEM images of SnO_x@C-G under **(c)** 10 , **(d)** 20 and **(e)** 30 min EUV radiation. **(f)** TEM image of SnO_x-G under 20 min EUV radiation.

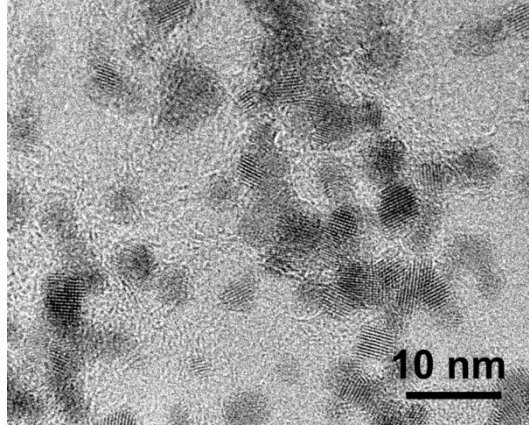


Fig. S8 HR-TEM image of SnO_x@C-G.

Fig. S8 shows discontinuous lattice fringes around the SnO_x nanoparticles. Although it is difficult to distinguish the carbon coating layer and the exfoliated graphite support at this resolution, the lattice fringes of the exfoliated graphite sheets can hardly be seen in the non-edge regions without folding (**Fig. S7b**). So it can be believed that these discontinuous lattice fringes are attributed to the carbon coating.

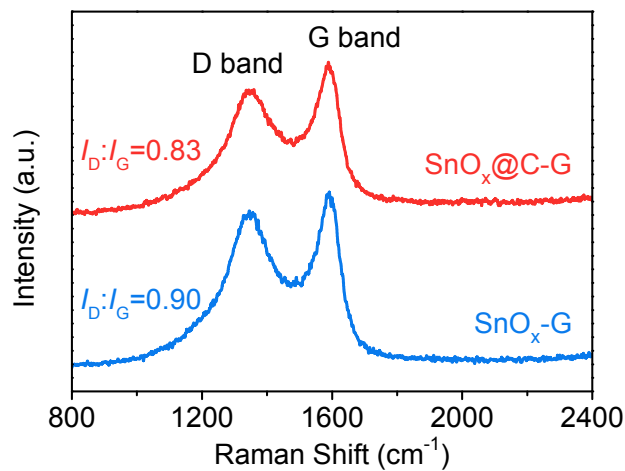


Fig. S9 Raman spectra of SnO_x@C-G and SnO_x-G.

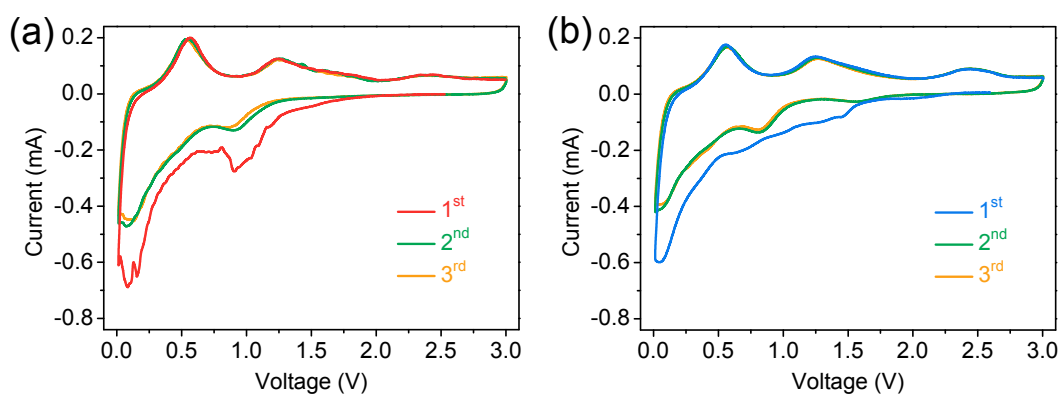


Fig. S10 Cyclic voltammogram (CV) curves of **(a)** SnO_x@C-G and **(b)** SnO_x-G electrode from 0.01 to 3 V vs. Li⁺/Li at a scan rate of 0.1 mV s⁻¹.

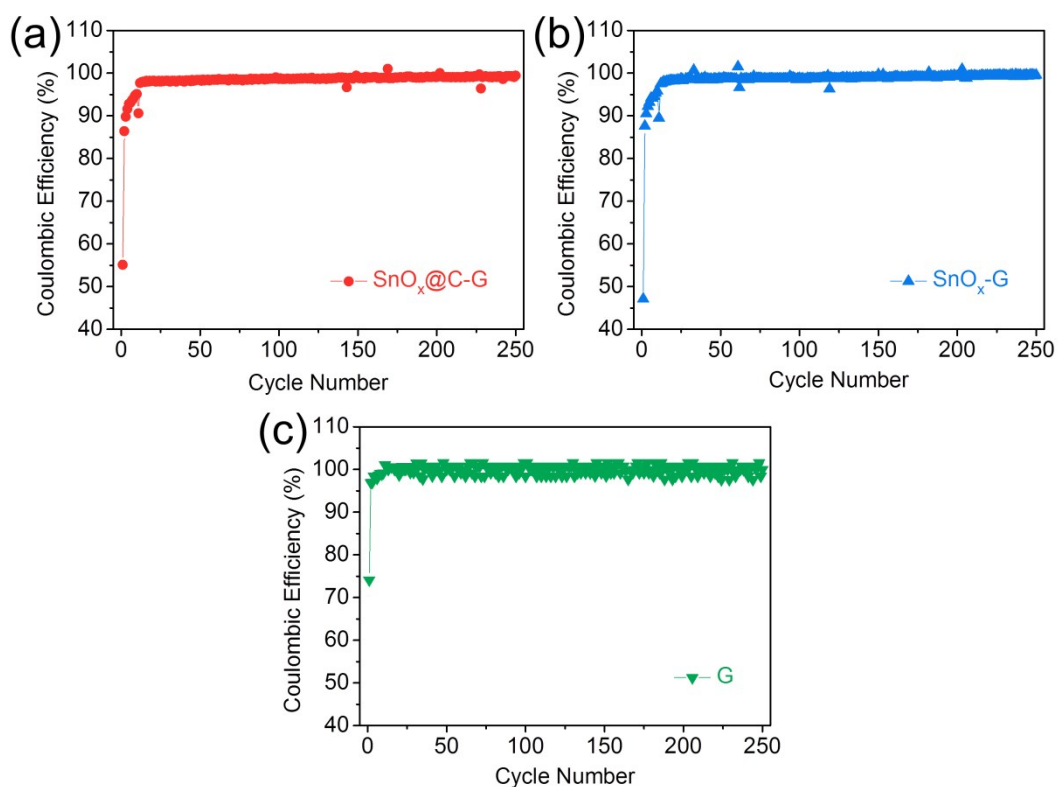


Fig. S11 Coulombic efficiency of **(a)** SnO_x@C-G, **(b)** SnO_x-G, and **(c)** exfoliated graphite electrode.

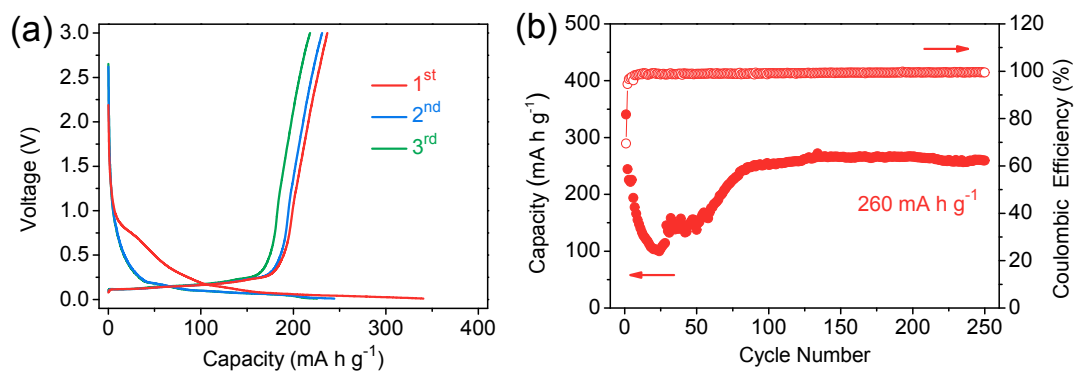


Fig. S12 (a) Galvanostatic charge/discharge profiles and **(b)** cycling performance of exfoliated graphite between 0.01 and 3.00 V at a current density of 0.1 A g⁻¹.

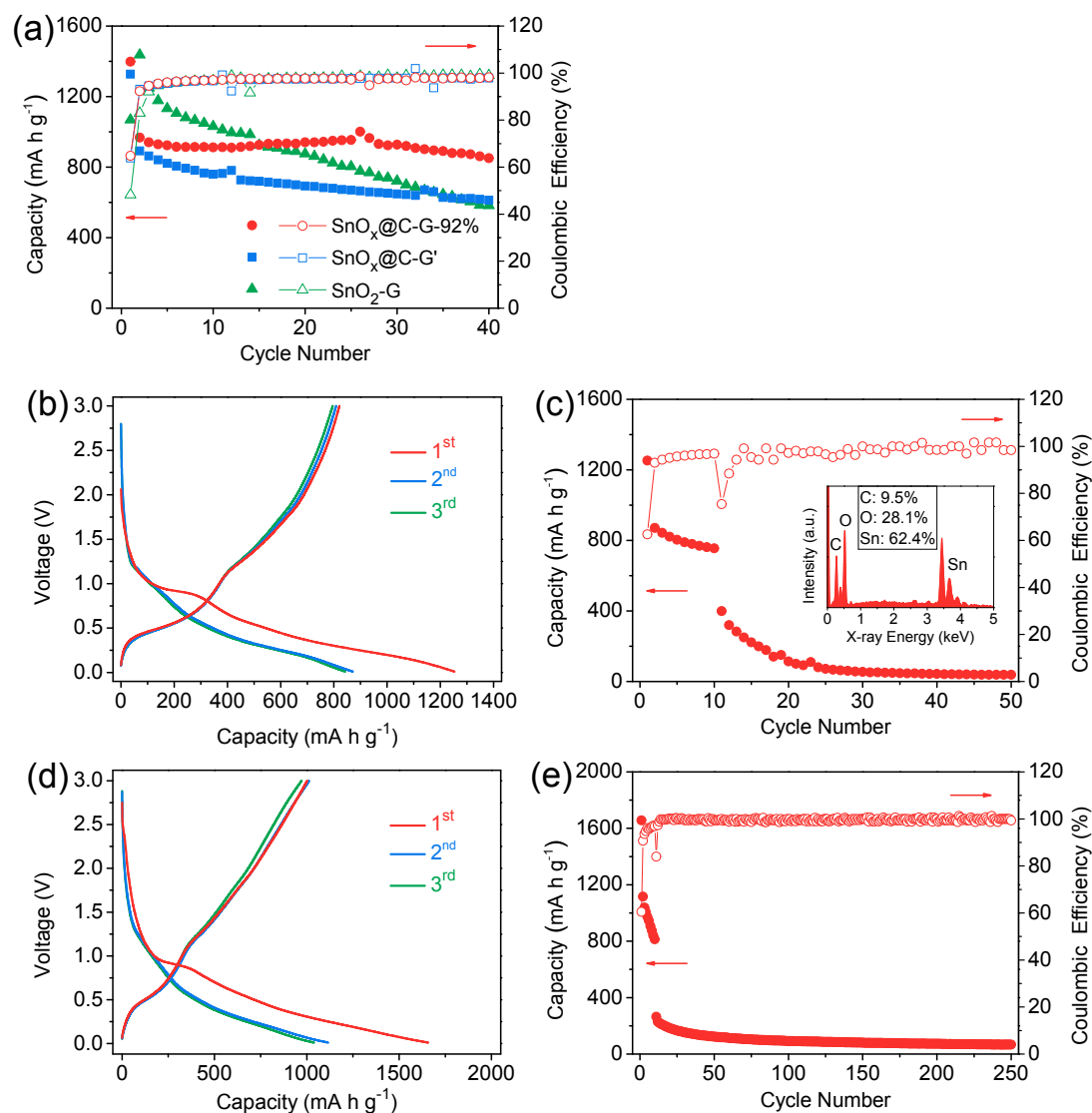


Fig. S13 (a) Cycling performances of $\text{SnO}_x\text{@C-G-92\%}$, $\text{SnO}_x\text{@C-G}'$ and $\text{SnO}_2\text{-G}$ between 0.01 and 3.00 V at a current density of 0.1 A g^{-1} . Galvanostatic charge/discharge profiles and cycling performances of $\text{SnO}_x\text{@C-G}'$ (**b, c**) and $\text{SnO}_2\text{-G}$ (**d, e**) at a current density of 0.1 A g^{-1} for the initial 10 cycles and 1.6 A g^{-1} for subsequent cycles.

The procedure to synthesize $\text{SnO}_x\text{@C-G-92\%}$ was the same as that of $\text{SnO}_x\text{@C-G}$. The $\text{SnO}_x\text{@C-G-92\%}$ anode was prepared with approx. 92% of $\text{SnO}_x\text{@C-G}$ and higher loading (approx. 6 mg cm^{-2}). The procedure to synthesize $\text{SnO}_x\text{@C-G}'$ was the same as that of $\text{SnO}_x\text{@C-G}$, but reduced the exfoliated graphite quality to 20 mg, and the EUV radiation was extended to 40 min. The ratio of SnO_x : exfoliated graphite is 4:1 calculated based on the EDS results in **Fig. S13c**. The $\text{SnO}_2\text{-G}$ with a mass ratio of

SnO₂: exfoliated graphite =1:1 was prepared by high energy ball milling with a rotating speed of 450 rpm for 4 h. Both of the two samples show the poor cycling stabilities at high current density of 1.6 A g⁻¹.

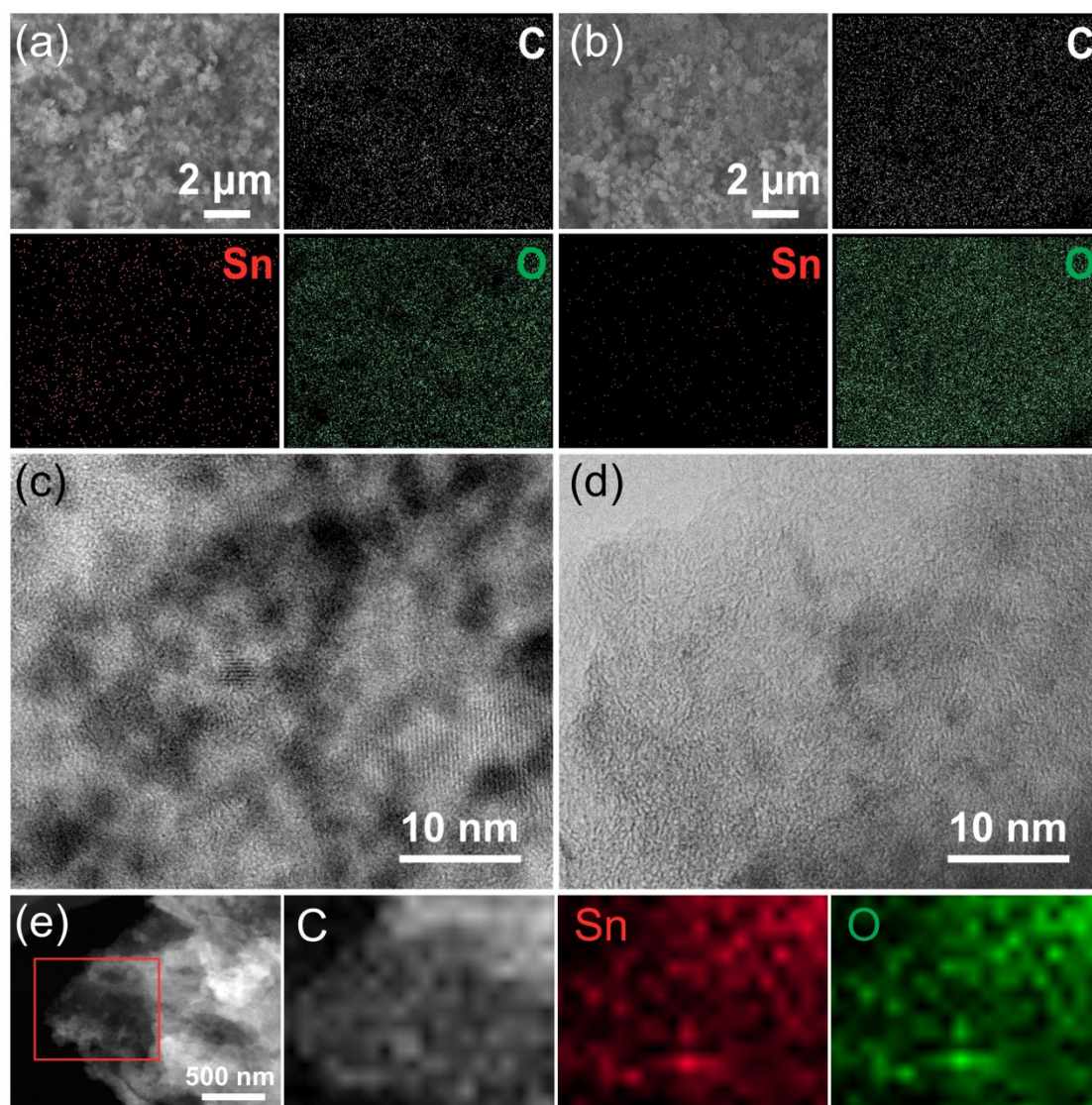


Fig. S14 Morphology and element distribution of SnO_x@C-G and SnO_x-G after 250 cycles. **(a)** SEM mapping and **(c)** TEM images of SnO_x@C-G. **(b)** SEM mapping and **(d)** TEM images of SnO_x-G. **(e)** STEM image and EDX mapping of SnO_x@C-G.

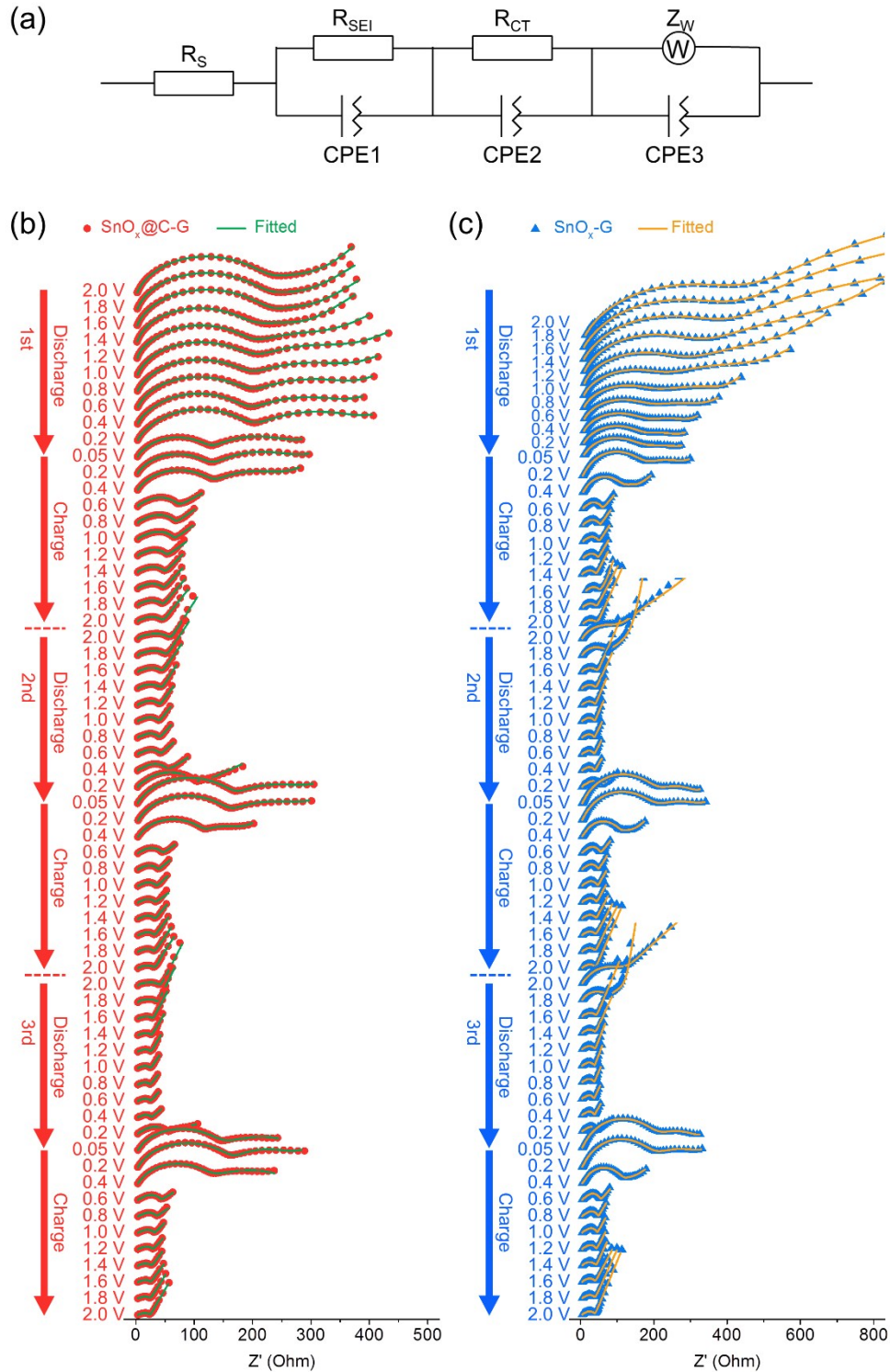


Fig. S15 (a) Equivalent circuit of $\text{SnO}_x\text{@C-G}$ and $\text{SnO}_x\text{-G}$ (R_s : electrolyte resistance, R_{SEI} : surface film resistance, R_{CT} : charge transfer resistance; CPE1–3: constant phase element, Z_w : Warburg impedance). Nyquist plots from in-situ EIS of **(b)** $\text{SnO}_x\text{@C-G}$ and **(c)** $\text{SnO}_x\text{-G}$ electrode with the fitted curves calculated by the above equivalent circuit.

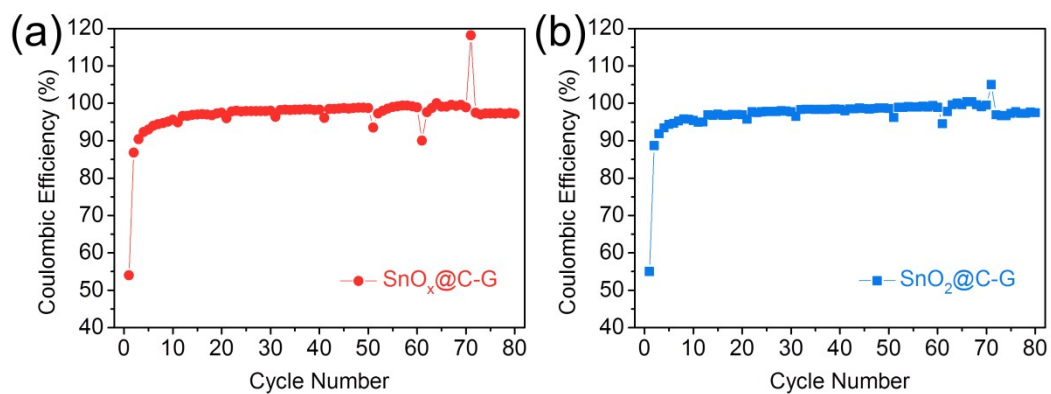


Fig. S16 Coulombic efficiency of (a) SnO_x@C-G and (b) SnO₂@C-G electrode corresponding to the rate performances.

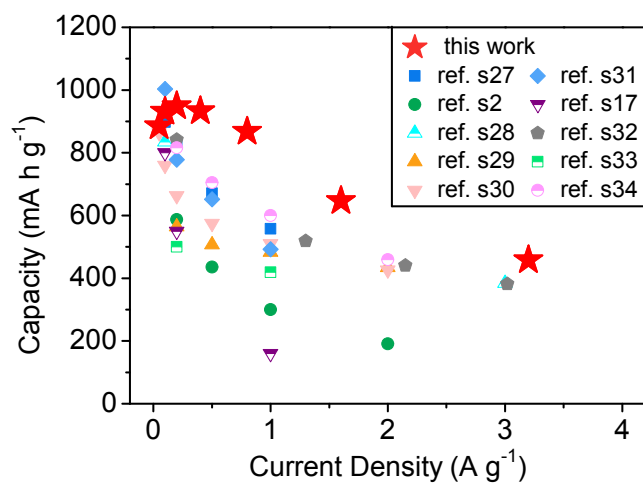


Fig. S17 Comparison of rate capacity with previous reported tin oxide/graphene material anodes.

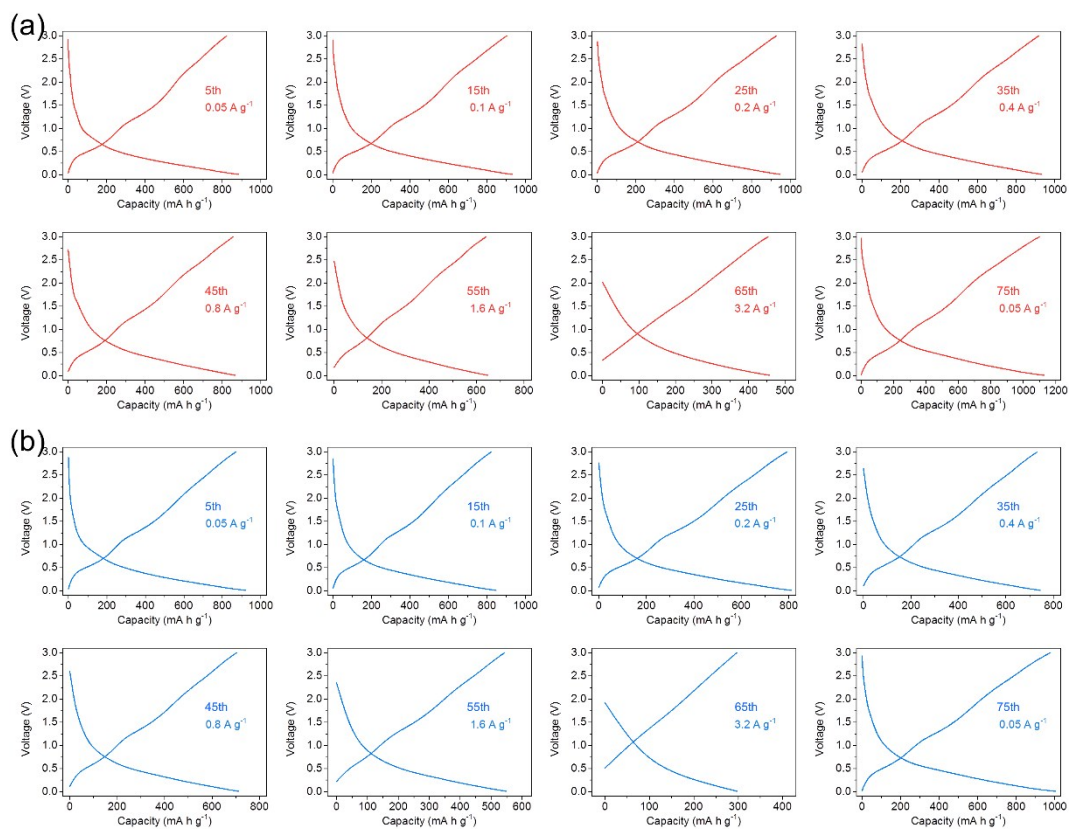


Fig. S18 The charge/discharge profiles of **(a)** $\text{SnO}_x\text{@C-G}$ and **(b)** $\text{SnO}_2\text{@C-G}$ electrode at varied current densities of 0.05–3.2 A g^{-1} .

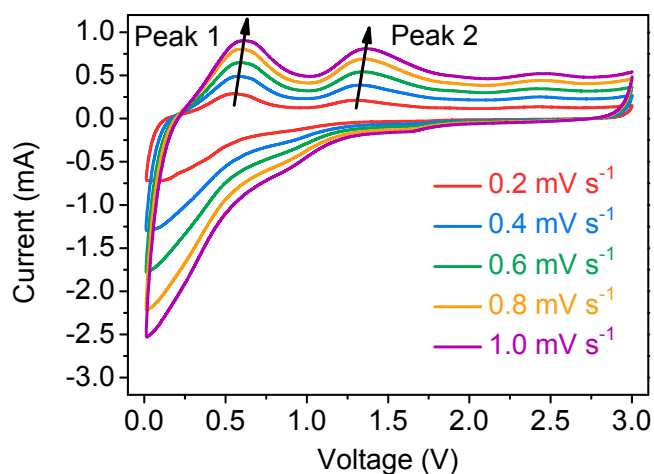


Fig. S19 CV results of the $\text{SnO}_2\text{@C-G}$ electrode recorded at increasing scan rates from 0.2 to 1.0 mV s^{-1} .

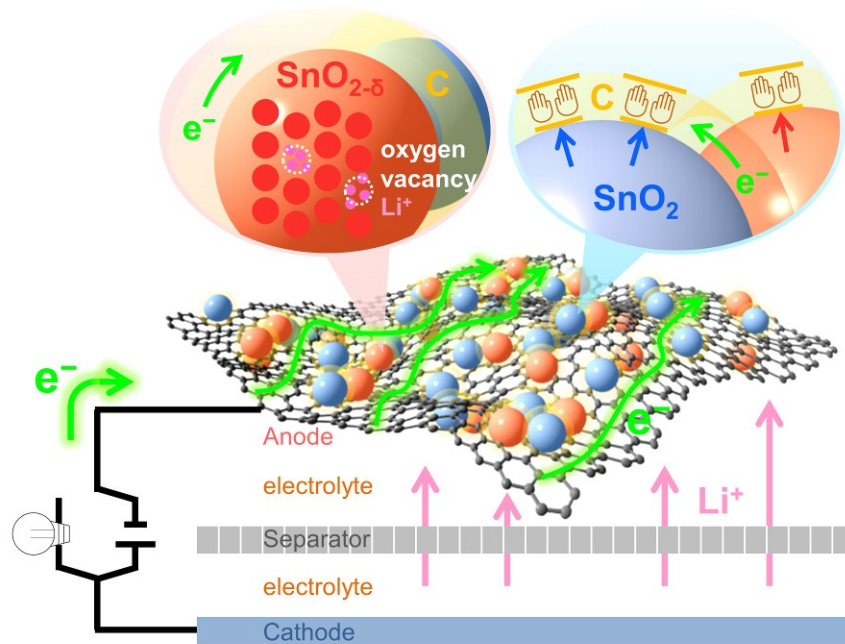


Fig. S20 Schematic illustration of mechanism of the capacitive effect and the protection of carbon coating in SnO_x@C-G as anode of lithium-ion batteries.

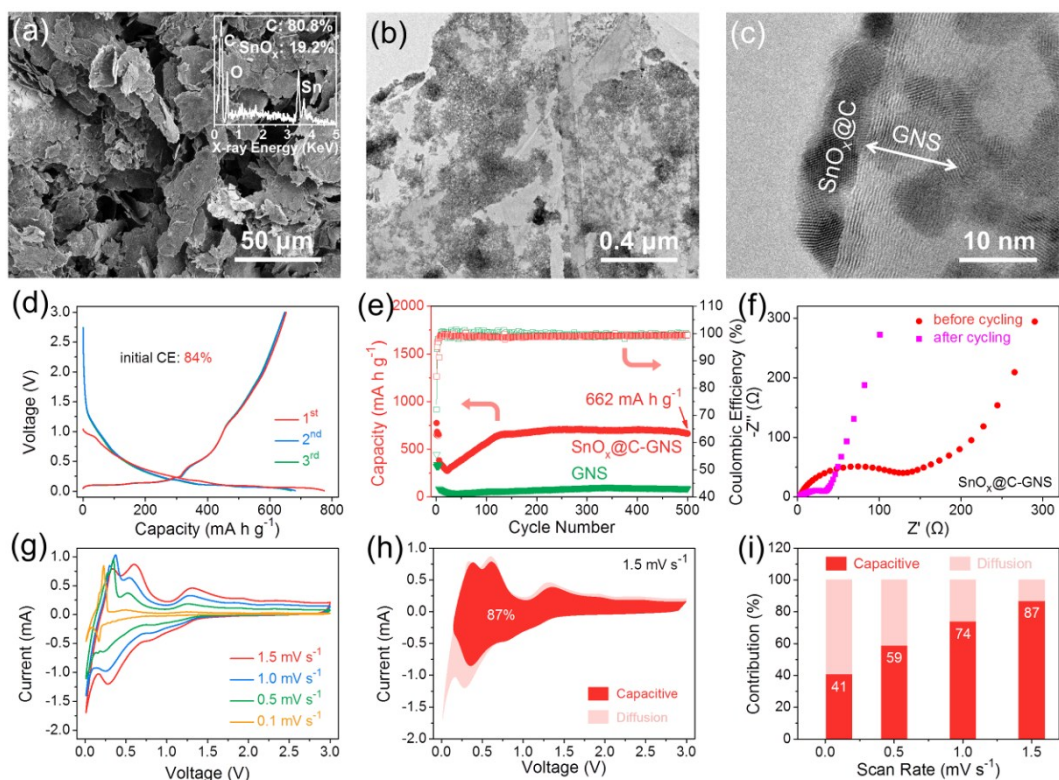


Fig. S21 (a) SEM image of $\text{SnO}_x\text{@C-GNS}$, insert: EDS spectrum. (b) TEM and (c) HR-TEM images of $\text{SnO}_x\text{@C-GNS}$. (d) Galvanostatic charge/discharge curves of the initial three cycles between 0.01 and 3.0 V at a current density of 0.1 A g^{-1} . (e) Cycling performances of $\text{SnO}_x\text{@C-GNS}$ and GNS at a current density of 0.1 A g^{-1} in the initial five cycles and 1.0 A g^{-1} in the subsequent cycles. (f) EIS spectra of $\text{SnO}_x\text{@C-GNS}$ before and after cycling measurements. (g) CV curves of the $\text{SnO}_x\text{@C-GNS}$ electrode recorded at increasing scan rates from 0.1 to 1.5 mV s^{-1} . (h) Charge storage contributions of $\text{SnO}_x\text{@C-GNS}$ from capacitive effects and diffusion-controlled process separated with CV at a scan rate of 1.5 mV s^{-1} . (i) Normalized contribution ratio of capacitive capacities at different scan rates.

Table S1. Cycling performance of SnO_x@C-G versus the reported tin oxide/graphene electrode materials at high current density ($\geq 1.0 \text{ A g}^{-1}$).

Sample	Voltage range (V)	Current density (A g^{-1})	Cycle number	Capacity (mA h g^{-1})	Reference
SnO _x @C-G	0.01–3	1.6	250	740	this work
SnO ₂ @P@GO	0.01–1	1.0	700	400	ref. s17
SnO _{2-x} /N-rGO	0.005–3	1.0	200	652	ref. s28
SnO ₂ @G-SWCNT50	0.001–3	1.0	300	537	ref. s29
FNT/S/RGO	0.01–3	1.0	1000	690	ref. s31
pG/SnO _x /C	0.01–3	1.0	400	555	ref. s33
ATO/N-GCA	0.005–3	1.0	1000	685	ref. s35
SnO ₂ /G-S	0.005–3	1.0	230	970	ref. s36
SnO ₂ @rGO	0.001–3	1.0	200	747	ref. s37
C@SnO ₂ -rGO-SnO ₂	0.01–3	2.0	1200	525	ref. s38
graphene/SnO ₂	0.01–3	1.0	250	445	ref. s39

References

- S1 K. Zhao, L. Zhang, R. Xia, Y. Dong, W. Xu, C. Niu, L. He, M. Yan, L. Qu and L. Mai, *Small*, 2015, **12**, 588.
- S2 M. Sahoo and S. Ramaprabhu, *Carbon*, 2018, **127**, 627.
- S3 F. Zoller, K. Peters, P. M. Zehetmaier, P. Zeller, M. Döblinger, T. Bein, Z. k. Sofer and D. Fattakhova-Rohlfing, *Adv. Funct. Mater.*, 2018, **28**, 1706529.
- S4 L. Fan, X. Li, B. Yan, J. Feng, D. Xiong, D. Li, L. Gu, Y. Wen, S. Lawes and X. Sun, *Adv. Energy Mater.*, 2016, **6**, 1502057.
- S5 W. Chen, K. Song, L. Mi, X. Feng, J. Zhang, S. Cui and C. Liu, *J. Mater. Chem. A*, 2017, **5**, 10027.
- S6 H.-P. Cong, S. Xin and S.-H. Yu, *Nano Energy*, 2015, **13**, 482.
- S7 L. Fenghua, S. Jiangfeng, Y. Huafeng, G. Shiyu, Z. Qixian, H. Dongxue, I. Ari and N. Li, *Nanotechnology*, 2009, **20**, 455602.
- S8 H. He, W. Fu, H. Wang, H. Wang, C. Jin, H. J. Fan and Z. Liu, *Nano Energy*, 2017, **34**, 449.
- S9 H. Song, N. Li, H. Cui and C. Wang, *J. Mater. Chem. A*, 2013, **1**, 7558.
- S10 C. Chen, L. Wang, Y. Liu, Z. Chen, D. Pan, Z. Li, Z. Jiao, P. Hu, C.-H. Shek, C. M. L. Wu, J. K. L. Lai and M. Wu, *Langmuir*, 2013, **29**, 4111.
- S11 J. Han, D. Kong, W. Lv, D.-M. Tang, D. Han, C. Zhang, D. Liu, Z. Xiao, X. Zhang, J. Xiao, X. He, F.-C. Hsia, C. Zhang, Y. Tao, D. Golberg, F. Kang, L. Zhi and Q.-H. Yang, *Nat. Commun.*, 2018, **9**, 402.
- S12 X. Sui, X. Huang, Y. Wu, R. Ren, H. Pu, J. Chang, G. Zhou, S. Mao and J. Chen, *ACS Appl. Mater. Interfaces*, 2018, **10**, 26170.
- S13 H. Xu, J. Chen, D. Wang, Z. Sun, P. Zhang, Y. Zhang and X. Guo, *Carbon*, 2017, **124**, 565.
- S14 Y. Huang, D. Wu, J. Wang, S. Han, L. Lv, F. Zhang and X. Feng, *Small*, 2014, **10**, 2226.
- S15 Z. Li, J. Ding, H. Wang, K. Cui, T. Stephenson, D. Karpuzov and D. Mitlin, *Nano Energy*, 2015, **15**, 369.
- S16 M. Zhang, Z. Sun, T. Zhang, D. Sui, Y. Ma and Y. Chen, *Carbon*, 2016, **102**, 32.
- S17 L. Zhang, K. Zhao, R. Yu, M. Yan, W. Xu, Y. Dong, W. Ren, X. Xu, C. Tang and L. Mai, *Small*, 2017, **13**, 1603973.
- S18 B. Chen, H. Qian, J. Xu, L. Qin, Q.-H. Wu, M. Zheng and Q. Dong, *J. Mater. Chem. A*, 2014, **2**, 9345.
- S19 J. Sun, L. Xiao, S. Jiang, G. Li, Y. Huang and J. Geng, *Chem. Mater.*, 2015, **27**, 4594.
- S20 J. Cui, S. Yao, J.-Q. Huang, L. Qin, W. G. Chong, Z. Sadighi, J. Huang, Z. Wang and J.-K. Kim, *Energy Storage Mater.*, 2017, **9**, 85.
- S21 Y. Wang, Y. Jin, C. Zhao, Y. Duan, X. He and M. Jia, *Mater. Lett.*, 2017, **191**, 169.
- S22 C. Zhu, S. Zhu, K. Zhang, Z. Hui, H. Pan, Z. Chen, Y. Li, D. Zhang and D.-W. Wang, *Sci. Rep.*, 2016, **6**, 25829.
- S23 W. Zhang, M. Li, X. Xiao, X. Huang, Y. Jiang, X. Fan and L. Chen, *J. Alloy Compd.*, 2017, **727**, 1.
- S24 X. Chu, J. Wang, J. Zhang, Y. Dong, W. Sun, W. Zhang and L. Bai, *J. Mater. Sci.*,

- 2017, **52**, 9441.
- S25 Y. Luo, S. Fan, Y. Luo, N. Hao, S. Zhong and W. Liu, *CrystEngComm*, 2015, **17**, 1741.
- S26 Y. Chen, B. Song, R. M. Chen, L. Lu and J. Xue, *J. Mater. Chem. A*, 2014, **2**, 5688.
- S27 S. Zuo, D. Li, Z. Wu, Y. Sun, Q. Lu, F. Wang, R. Zhuo, D. Yan, J. Wang and P. Yan, *Electrochim. Acta*, 2018, **264**, 61.
- S28 N. Wu, W. Du, X. Gao, L. Zhao, G. Liu, X. Liu, H. Wu and Y.-B. He, *Nanoscale*, 2018, **10**, 11460.
- S29 J. Wang, F. Fang, T. Yuan, J. Yang, L. Chen, C. Yao, S. Zheng and D. Sun, *ACS Appl. Mater. Interfaces*, 2017, **9**, 3544.
- S30 Q. Shao, J. Tang, Y. Sun, J. Li, K. Zhang, J. Yuan, D. M. Zhu and L. C. Qin, *Nanoscale*, 2017, **9**, 4439.
- S31 K. Lee, S. Shin, T. Degen, W. Lee and Y. S. Yoon, *Nano Energy*, 2017, **32**, 397.
- S32 C. Miao, M. Liu, Y.-B. He, X. Qin, L. Tang, B. Huang, R. Li, B. Li and F. Kang, *Energy Storage Mater.*, 2016, **3**, 98.
- S33 D. Zhou, W.-L. Song, X. Li and L.-Z. Fan, *ACS Appl. Mater. Interfaces*, 2016, **8**, 13410.
- S34 H. Tao, S. Zhu, L. Xiong, X. Yang and L. Zhang, *ChemElectroChem*, 2016, **3**, 1063.
- S35 J. Cui, S. Yao, J.-Q. Huang, L. Qin, W. G. Chong, Z. Sadighi, J. Huang, Z. Wang and J.-K. Kim, *Energy Storage Mater.*, 2017, **9**, 85.
- S36 W. Chen, K. Song, L. Mi, X. Feng, J. Zhang, S. Cui and C. Liu, *J. Mater. Chem. A*, 2017, **5**, 10027.
- S37 S. Shi, T. Deng, M. Zhang and G. Yang, *Electrochim. Acta*, 2017, **246**, 1104.
- S38 W. Yao, S. Wu, L. Zhan and Y. Wang, *Chem. Eng. J.*, 2019, **361**, 329.
- S39 X. Liu, T. Ma, L. Sun, Y. Xu, J. Zhang and N. Pinna, *ChemSusChem*, 2018, **11**, 1321.